ACS OMEGA

http://pubs.acs.org/journal/acsodf

Article

Co-Gasification Synergistic Characteristics of Sewage Sludge and High-Sodium Coal

Zhiyuan Zhang, Lilin Zhang,* Yin Liu, Mingxu Lv, Peibo You, Xutao Wang, Hengtao Zhou, and Jing Wang

Cite This: *ACS Omega* 2023, 8, 6571−6583

Read Online

ACCESS | Metrics & More | Article Recommendations

ABSTRACT: A comprehensive study was conducted to assess the co-gasification characteristics of sewage sludge and high-sodium coal. As the gasification temperature increased, the CO_2 concentration was decreased, and the concentrations of CO and H_2 were increased, while the change of CH_4 concentration was not obvious. As the coal blending ratio increased, the H_2 and CO concentrations initially increased and then decreased, while the CO_2 concentration initially decreased and then increased. The mixture of sewage sludge and high-sodium coal shows the synergistic effect of co-gasification, and the synergistic effect was to promote the gasification reaction positively. The average activation energies of co-gasification reactions were calculated by the OFW method, and the average activation energy initially decreases and then increases as the coal blending ratio increases. Both fluidized-bed gasification and thermogravimetric analyzer gasification show that the optimum coal blending ratio is 0.6. Overall, these results provide a theoretical basis for the industrial application of sewage sludge and high-sodium coal co-gasification.

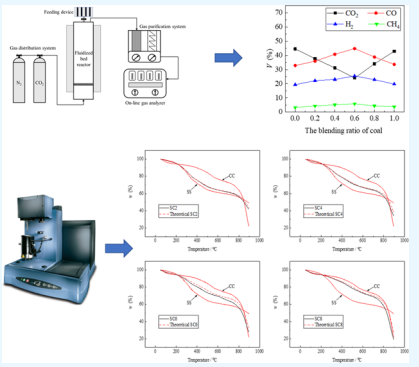

1. INTRODUCTION

Sewage sludge is a byproduct generated in the process of sewage treatment, which contains many organic pollutants, heavy metals, parasites, pathogens, and other substances harmful to the environment and human health.[1−4] Due to rapid economic and social developments globally, the quantity of sludge produced has dramatically increased. Many countries have developed relevant policies regarding sludge treatment and disposal to encourage a reduction in its yield in a controllable way and render it harmless, with an eye toward transformation to useful products. Due to high levels of organic matter and combustible components, dry sludge has a high calorific value and exhibits great potential for energy utilization.[5−7] This utilization of sewage sludge is of great significance as it not only realizes environmentally friendly sludge disposal but also captures the energy contained within the sewage sludge.

Technologies for energy utilization of sewage sludge include combustion, pyrolysis, and gasification. Sewage sludge combustion significantly reduces the sludge volume but produces hazardous gases such as SO_2 and NOx.[8,9] Sewage sludge pyrolysis, carried out in an oxygen-free or anoxic high-temperature environment, produces less harmful gases but does not maximize the reduction of sludge volume.[10,11] Sewage sludge gasification converts the organic components in sludge into combustible gas, which has the advantages of less harmful gas emission and significant volume reduction effect.[12−14] Therefore, sewage sludge gasification is an effective way for the efficient resource utilization of sludge.

In virtue of its great application potential, sewage sludge gasification has been intensively studied. Viswanathan et al.[15] investigated the thermochemical conversion of sewage sludge through a downdraft gasifier, proposed the two-zone equilibrium and one-zone kinetic model as the mixed model of sludge gasification, and found that the composition of syngas and the cold gas efficiency were greatly affected by the temperature and pressure of the gasifier as well as the inlet flow of the gasification agent and the raw material. Migliaccio et al.[12] reported the gasification characteristic of sewage sludge at different values of oxygen/fuel equivalence ratios in a bench-scale fluidized-bed reactor, analyzed the influence of seasonal fluctuations of sludge chemical composition on the gasification products, and considered that a higher oxygen/fuel equivalence ratio can reduce the tar yield, and the surface area of the bottom ash produced by gasification in a more reducing atmosphere is relatively high. Yan et al.[16] studied the effects of K_2CO_3 and biomass ash on sludge gasification and found that after

Received: October 28, 2022
Accepted: January 20, 2023
Published: February 9, 2023

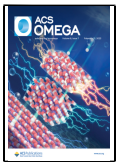

https://doi.org/10.1021/acsomega.2c06962
ACS Omega 2023, 8, 6571−6583

Table 1. Proximate and Ultimate Analyses of the Samples[a]

	proximate analysis (%)				$Q_{ad,net}$ (MJ·kg^{-1})	ultimate analysis (%)				
sample	M_t	A_{ad}	V_{ad}	FC_{ad}		C_{ad}	H_{ad}	O_{ad}	N_{ad}	S_{ad}
sludge	5.64	40.16	42.27	12.55	12.95	32.35	5.37	13.87	2.69	0.65
coal	6.85	5.57	30.18	57.87	22.35	69.27	4.93	12.85	0.84	0.34

[a]M_t, total moisture; A, ash; V, volatile matter; FC, fixed carbon; ad, air-dried basis.

Table 2. Ash Compositions of the Samples

	ash compositions (%)									
sample	SiO_2	Al_2O_3	Fe_2O_3	CaO	MgO	TiO_2	SO_3	K_2O	Na_2O	P_2O_5
sludge	26.37	16.46	10.66	21.75	2.72	0.42	5.42	1.66	2.74	9.52
coal	14.53	8.13	3.92	39.72	6.83	0.66	18.78	0.64	5.39	0.17

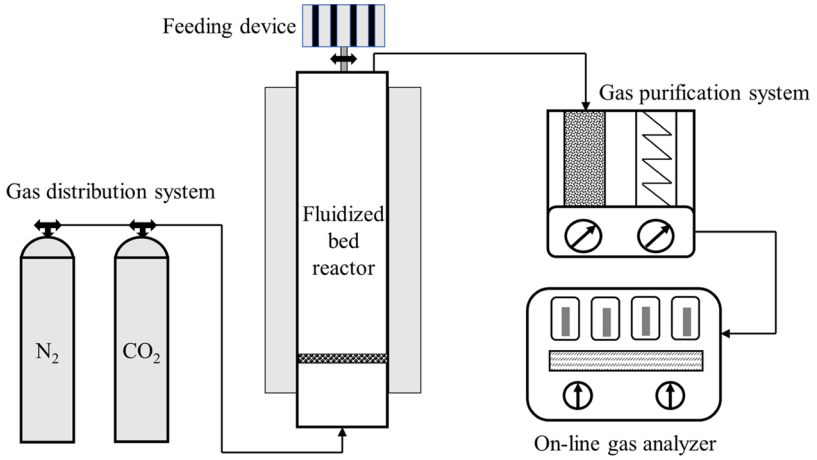

Figure 1. Experimental system of fluidized-bed gasification.

introducing steam into the simulated real flue gas, the low calorific value reached twice that without steam, and K_2CO_3 was conducive to promoting the formation of CO.

To date, extensive studies on sewage sludge gasification have been reported, but due to the low calorific value of sewage sludge, the calorific value of combustible gas produced during gasification is low, which is not conducive to subsequent utilization. However, the co-gasification of sludge and coal, biomass, or other high-calorific-value fuels can improve the calorific value of gas products, which is more satisfactory for industry applications.

Zhang et al.[17] researched the co-gasification characteristic of bituminous coal and sludge in a downdraft fixed-bed gasifier and found that the increase of gasification temperature can improve the syngas content, the gasification performance as well as the contents of H_2 and CO, and the gasification performance reduced as the air equivalent ratio increased, and the highest cold gas efficiency was obtained when the coal blending ratio was 0.7. Rosha et al.[18] discussed the technical feasibility of co-gasification of biomass and paper-mill sludge and used Aspen Plus to obtain the optimal conditions for maximizing the yield of the H_2 gasification product. Stanislaw et al.[19] investigated the co-gasification of sewage sludge and Virginia Mallow and found that the presence of Virginia Mallow helps stabilize and promote the gasification process, which produces syngas with a calorific value of about 5 MJ·Nm^{-3}.

High-sodium coal is prone to contamination and slagging during direct combustion and utilization, which hinders the efficient utilization of high-sodium coal.[20,21] However, the sodium element in high-sodium coal has a catalytic effect on the gasification process.[22] Therefore, co-gasification of sewage sludge and high-sodium coal is conducive to the energy utilization of sludge, improving the calorific value of combustible gas, and providing a new way for the clean and efficient utilization of high-sodium coal.

Scholars have carried out some research on the co-gasification characteristics of sludge and high-calorific-value fuels; however, regarding the co-gasification characteristics of sewage sludge and high-sodium coal, satisfactory conditions for effective gasification have seldom been studied. Therefore, the purpose of this paper is to systematically investigate the co-gasification synergistic characteristics of sewage sludge and high-sodium coal. The effects of the coal blending ratio and gasification temperature were investigated in an electrically heated fluidized bed. The co-gasification reaction characteristics were analyzed by a thermogravimetric analyzer, and the activation energies of co-gasification reactions were calculated by the Ozawa−Flynn−Wall method. The findings of this study will help explore a new way of efficient energy utilization of sewage sludge and high-sodium coal.

2. MATERIALS AND METHODS

2.1. Sample Preparation. The sewage sludge used was activated sludge, which came from a sewage treatment plant in Urumqi City, China. The coal used was high-sodium coal, which came from the Zhundong region of Xinjiang, China. The raw materials were initially dried in a 100 °C vacuum drying oven until there was no obvious change in weight. After cooling to

https://doi.org/10.1021/acsomega.2c06962
ACS Omega 2023, 8, 6571−6583

room temperature, the dried sewage sludge and high-sodium coal were crushed and ground separately, and the powder with a particle size of 0.10−0.15 mm was selected as the experimental sample.

The proximate and ultimate analyses of dried sewage sludge powder and high-sodium coal powder were performed using a proximate analyzer (ECA-3, Thermo Scientific) and a CHN/O/S elemental analyzer (EA 2400, PerkinElmer), respectively. The low calorific value was performed using a bomb calorimeter (Parr 6300, Parr Instrument). Table 1 shows the proximate and ultimate analyses of the sewage sludge powder and the high-sodium coal powder used in the experiments. Table 2 shows the ash composition of sewage sludge and high-sodium coal.

The sewage sludge powder and high-sodium coal powder were fully mixed according to the mass ratios of 10:0, 8:2, 6:4, 4:6, 2:8, and 0:10 separately. For the convenience of research, the above samples were named SS, SC2, SC4, SC6, SC8, and CC, respectively.

In addition, to further compare the influence of ash in high-sodium coal on gasification, the ash-free sample of high-sodium coal was prepared as follows. CC was mixed with 1.0 mol L^{-1} hydrochloric acid at a temperature of 60 °C for 24 h, and the CC/hydrochloric acid ratio (w/v) was fixed during the experiments at 1 g: 25 mL. Then, the solid residues were washed with deionized water three times. Finally, the solid residues were dried at 98 °C until there was no detailed change in mass, which was denoted as CC-AF.

2.2. Fluidized-Bed Gasification Experiments. The experimental system of fluidized-bed gasification is shown in Figure 1. The system consists of a gas distribution system, an electrically heated fluidized-bed reactor, a feeding device, a gas filter, and an online gas analyzer.

The electrically heated fluidized-bed reactor is composed of a fluidized-bed reaction chamber and an electric heater wrapped around the reaction chamber. The fluidized-bed reaction chamber was a quartz tube (inner diameter: 40 mm; height: 1400 mm), and an air distribution plate was set at 600 mm at the bottom of the tube to uniform the flow field. The temperature of the fluidized-bed reactor is controlled by the temperature control module on the electric heater, and the control accuracy is ±1 °C.

The concentrations of gas product components were measured by an online gas analyzer (Gasboard 3100, Ruiyi, China). The principle of this gas analyzer for measuring CO/CO_2/CH_4 is nondispersive InfraRed, and the measurement error is ±1%F.S. The principle for measuring H_2 detection is the thermal conductivity detector, and the measurement error is ±2%F.S.

The feeding device was controlled by a magnetic valve. After calibration, the error of fuel supply is ±0.01 g/min. In addition, all experiments were repeated three times to ensure accuracy.

For each experimental run, the fluidized-bed reactor was heated to the experimental temperature by the temperature control module, and the sample was then fed into the fluidized-bed reaction reactor by the feeding device at the speed of 1 g·min^{-1}. CO_2 was used as the gasification medium, and N_2 was used as the carrier, in which CO_2 flow was 1 L·min^{-1} and the fluidization number was 5. The stabilization time of each experiment was about 1 min, while the duration of the whole experiment was about 5 min. In this process, the sample was continuously fed into the reactor and remained until the experiment stopped. After the experiment was stopped and the temperature was cooled to room temperature, the ash in the reactor was collected and cleaned.

2.3. Thermogravimetric Gasification Experiments. The thermogravimetric gasification experiments were carried out on a TGA (Q50, TA Instruments). Blank experiments were carried out to obtain the empty crucible measurement baselines. The blank baselines were deducted from the experimental results to eliminate the influence of buoyancy factors under each experimental condition, and the real and accurate weight loss information was obtained from the samples.

For each experimental run, 10 mg of sample was weighed and evenly spread in an alumina crucible, and then, the reaction chamber was closed. Ultrapure N_2 (99.999%) was introduced at a flow rate of 60 mL min^{-1} for 15 min to purge the TGA instrument. Then, the sample was heated from 50 °C to the final temperature in a CO_2 atmosphere at a specified heating rate.

2.4. Co-Gasification Reaction Kinetics. To express the gasification conversion degree of the sample, the gasification conversion rate (α) of the sample was defined as

$$\alpha = \frac{m_0 - m}{m_0 - m_a} \tag{1}$$

where α is the gasification conversion rate, %; m_0 is the initial mass of the sample, mg; m is the sample mass at time t, mg; and m_a is the sample mass at the end of the gasification reaction, mg.

The kinetic equation of the gasification reaction follows the general equation of the gas−solid reaction

$$\frac{d\alpha}{dt} = kf(\alpha) \tag{2}$$

where $f(\alpha)$ is the gasification reaction mechanism function, which is mainly determined by reaction type or reaction mechanism; k is the reaction rate constant; and t is the reaction time, s.

The reaction rate constant (k) follows the Arrhenius law

$$k = Ae^{E/RT} \tag{3}$$

where T is the reaction temperature, K; A is the pre-exponential factor, s^{-1}; E is the activation energy, kJ mol^{-1}; and R is the universal gas constant.

The heating rate (β) can be expressed as follows

$$\beta = \frac{dT}{dt} \tag{4}$$

where β is the heating rate, K·min^{-1}; T is the reaction temperature, K; and the reaction time, min.

Combining eqs 3, 4 with 2, eq 5 was obtained

$$\frac{d\alpha}{dT} = \frac{A}{\beta}e^{-E/RT}f(\alpha) \tag{5}$$

Using the traditional single heating rate method, it was difficult to ensure the rationality of the selected reaction mechanism function. Therefore, the model-free method was used to calculate the activation energy of the co-gasification reaction in this research. The model-free method was used to carry out co-gasification kinetic analysis according to the thermal analysis curves obtained at different heating rates, which could separate the reaction mechanism function, and the reliable value of activation energy was obtained without introducing the kinetic model function.[23,24]

The calculation of activation energy was carried out using the Ozawa−Flynn−Wall (OFW) method[25,26]

https://doi.org/10.1021/acsomega.2c06962
ACS Omega 2023, 8, 6571−6583

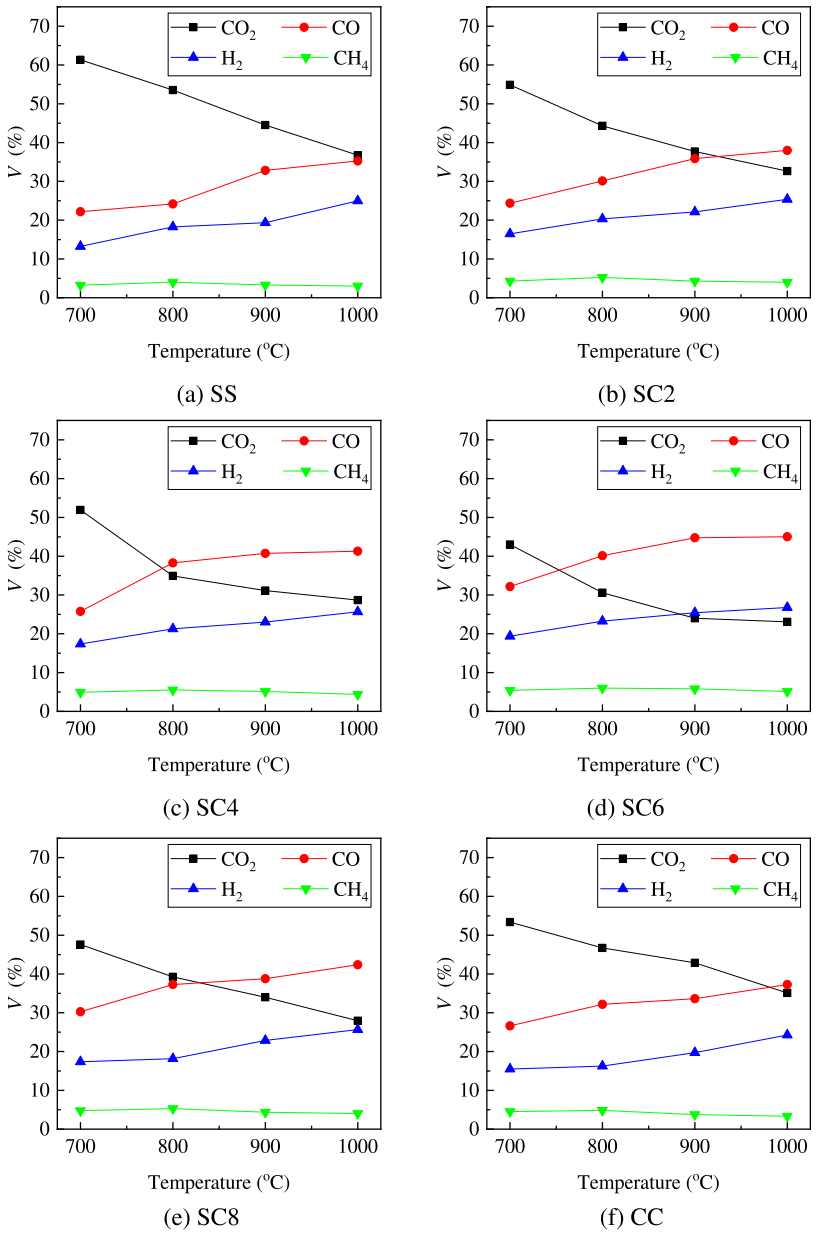

Figure 2. Relationship between gas concentration and temperature at different blending ratios: (a) sample of SS; (b) sample of SC2; (c) sample of SC4; (d) sample of SC6; (e) sample of SC8; and (f) sample of CC.

$$\ln(\beta) = \ln\left(\frac{AE}{Rf(\alpha)}\right) - 5.331 - 1.052\frac{E}{RT} \quad (6)$$

According to different heating rates and a given α, a linear relationship was observed by plotting $\ln(\beta)$ vs T^{-1}, and E was calculated by the slope. During the experiment, different heating rates were controlled by TGA, and then, the value of E was obtained.

3. RESULTS AND DISCUSSION

3.1. Effects of Gasification Temperature on Co-Gasification. The gas components in the gasification process mainly include CO_2, CO, H_2, CH_4, and C_aH_{a+2} ($2 \le a \le 4$). Generally, the yield of C_aH_{a+2} is very low, so only CO_2, CO, H_2, and CH_4 gases are discussed. The gasification experiment of each sample at different reaction temperatures was carried out in the fluidized-bed system, and the gas components produced at different gasification temperatures are shown in Figure 2.

As the gasification temperature increased, all samples showed a decrease in the CO_2 concentration and an increase in the concentrations of CO and H_2, while the change of CH_4 concentration was not obvious.

In the CO_2 gasification reaction, the following key reactions are mainly involved.

$$C_xH_yO_z \rightarrow C + CO + CO_2 + C_mH_n + H_2 + H_2O - Q_1 \quad (7)$$

$$C + CO_2 \rightarrow CO - Q_2 \quad (8)$$

$$C_mH_n + CO_2 \rightarrow CO + H_2 - Q_3 \quad (9)$$

$$C + H_2 \rightarrow CH_4 + Q_4 \quad (10)$$

https://doi.org/10.1021/acsomega.2c06962
ACS Omega 2023, 8, 6571−6583

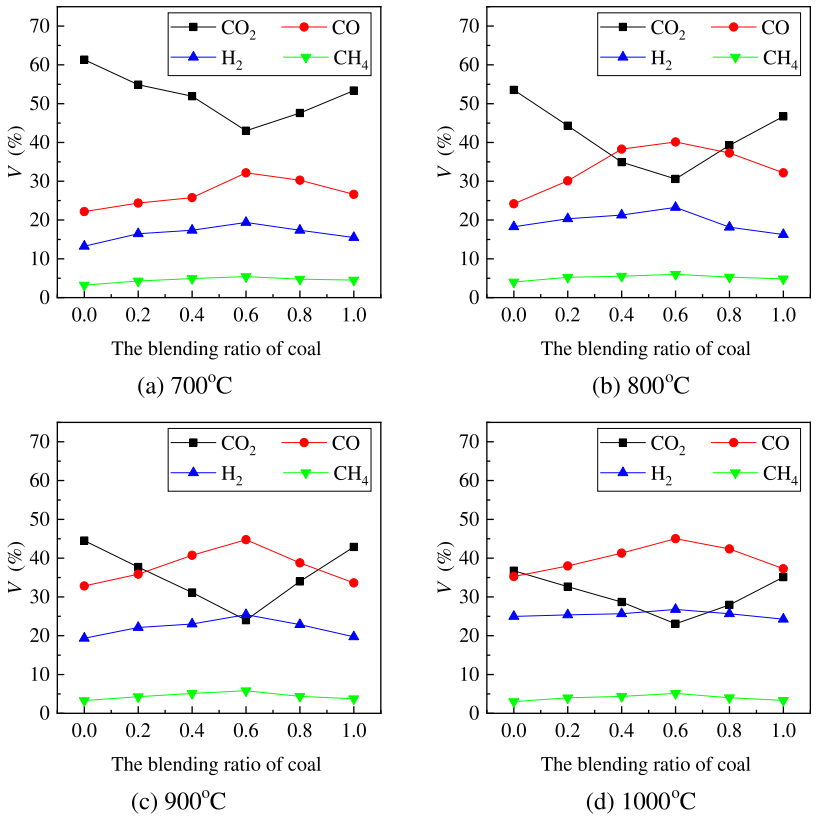

Figure 3. Relationship between gas concentration and coal blending ratio at different temperatures: (a) 700 °C, (b) 800 °C, (c) 900 °C, and (d) 1000 °C.

It can be seen that reactions eqs 7,8, and 9 are endothermic reactions, while reaction eq 10 is an exothermic reaction. The increase of gasification temperature provides more energy for the gasification process and can promote the progress of reactions 7,8, and 9. Reactions 8 and 9 need to consume CO_2 and produce CO and H_2. Therefore, it is detected that the CO_2 concentration decreases with the increase of gasification temperature, while the CO and H_2 concentration increases with the increase of gasification temperature. Reaction 10 is an exothermic reaction, and the rise of the gasification temperature inhibits the forward progress of this reaction, so the CH_4 concentration remains basically unchanged.

3.2. Effect of Coal Blending Ratio on Co-Gasification.

Figure 3 shows the relationship between gas concentration and the coal blending ratio at different temperatures. As the coal blending ratio increased, the samples at different temperatures showed that H_2 and CO concentrations initially increased and then decreased, while the CO_2 concentration initially decreased and then increased.

It shows that the addition of high-sodium coal into sludge promotes the gasification reaction at different gasification temperatures, and the influence of the coal blending ratio on the CO volume is more significant. At 800 °C, the CO volume can be increased from 24.18 to 40.12% by adjusting the coal blending ratio, while the volume of H_2 can only be increased from 19.35 to 25.44%.

To further evaluate the energy conversion in the gasification process, the cold gas efficiency (η) was defined as follows[27,28]

$$\eta = \frac{V_{CO} \times Q_{co} + V_{H_2} \times Q_{H_2} + V_{CH_4} \times Q_{CH_4}}{M_{fuel} \times Q_{fuel}} \times 100\% \quad (11)$$

where V_{co}, V_{H_2}, and V_{CH_4} are the volumes of CO, H_2, and CH_4, respectively, m^3; Q_{co}, Q_{H_2}, and Q_{CH_4} are the low calorific values of CO, H_2, and CH_4, respectively, $kJ \cdot m^{-3}$; M_{fuel} is the total mass of the experimental sample, kg; Q_{fuel} is the low calorific value of the experimental sample, which can be converted from the low calorific value of sewage sludge and high-sodium coal according to the coal blending ratio, $kJ \cdot kg^{-1}$.

Figure 4 shows the variation of cold gas efficiency with temperature and the coal blending ratio. As the temperature

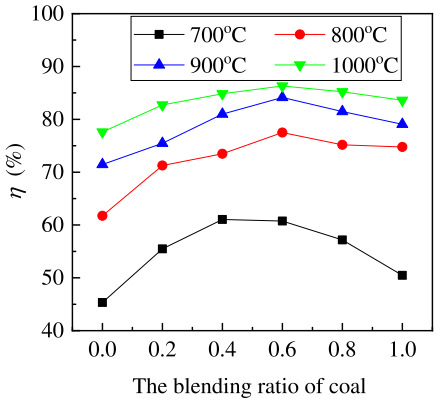

Figure 4. Variation of cold gas efficiency with temperature and coal blending ratio.

https://doi.org/10.1021/acsomega.2c06962
ACS Omega 2023, 8, 6571−6583

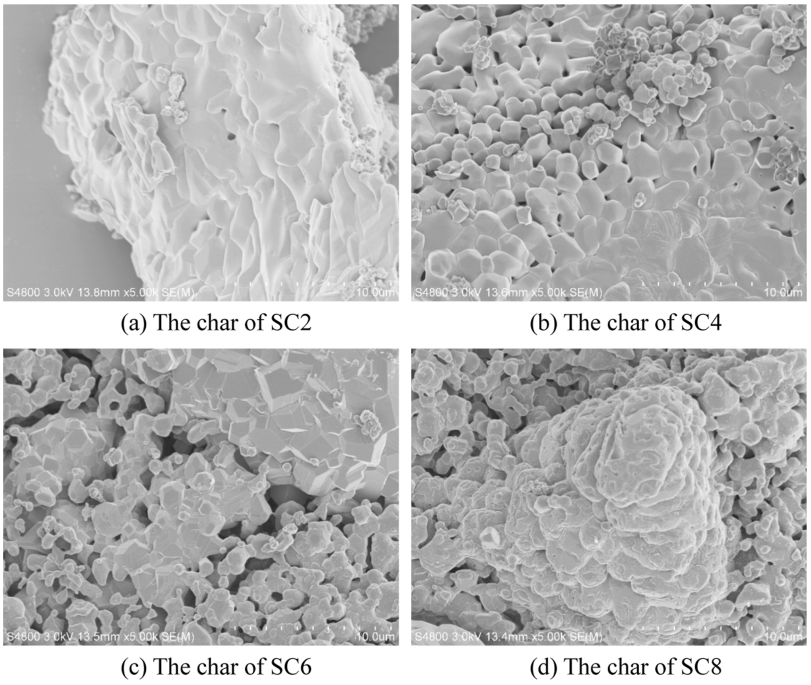

Figure 5. Morphological characteristics of char samples: (a) char of SC2, (b) char of SC, (c) char of SC6, and (d) char of SC8.

increased, the cold gas efficiency of all samples increased gradually, and the higher the temperature, the less obvious the synergistic gasification effect of sewage sludge and high-sodium coal. Moreover, the cold gas efficiency at different temperatures reaches the maximum at the coal blending ratio of 0.6. Zou et al.[29] also found that there is an optimal proportion of oil sludge and coal to achieve the optimal gasification reaction.

To further analyze the mechanism of the optimal mixing ratio of sludge and coal, the morphological characteristics of char samples with different coal blending ratios were obtained using a scanning electron microscope (SEM, Hitachi S-4800, Japan), as shown in Figure 5. It can be seen that the surface pore structure of char is less when the blending ratio of coal is 0.2. With the increase of the blending ratio of coal, a more abundant pore structure is formed in char, which can improve the gasification reactivity. However, when the blending ratio of coal reaches 0.8, pore plugging occurs on the char surface, which reduces the gasification reactivity.

3.3. Co-Gasification Characteristics under Temperature Programmed. To further analyze the co-gasification synergistic characteristics of sewage sludge and high-sodium coal, the samples were heated from 50 to 900 °C at the heating rate of 10 K·min^{-1}, and the experimental TG curves of the samples were obtained.

The TG curves of CC and CC-AF are shown in Figure 6. It can be seen that after deashing of high-sodium coal with hydrochloric acid, under the same reaction conditions, the gasification reaction capacity of deashing coal is significantly reduced compared with that before deashing. This fully shows that the ash content in high-sodium coal, especially the sodium element, can promote gasification.

This phenomenon is mainly because sodium can inhibit the evolution of coal char to graphitization in the process of thermal condensation, promote a high degree of disorder of the coal char microcrystalline structure, and facilitate the gasification reaction. In addition, sodium can erode and slot the surface of coal char particles during the gasification reaction, increasing the surface

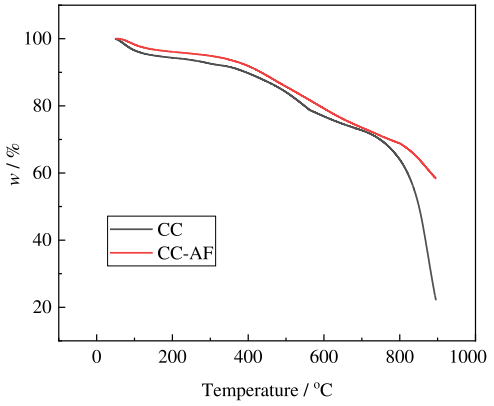

Figure 6. TG curves of CC and CC-AF.

active sites and active surface area of coal char, and thus promoting the gasification reaction.[21,22]

The theoretical TG curves of the samples were calculated according to the experimental TG curve of SS and CC by the weighted average method,[30] as shown in Figure 7. It can be seen that different coal blending ratios lead to different TG curves of samples, but the change trend of the whole gasification process is basically the same, which can be divided into three stages: drying desorption stage (50−250 °C), slow gasification stage (250−750 °C), and fast gasification stage (750−900 °C). For samples with different coal blending ratios, at the same time point, the experimental weight loss is greater than the theoretical weight loss, which reflects the synergistic effect of co-gasification, and the gasification synergistic effect of samples with different coal blending ratios is also different.

The synergy of the four samples in the drying desorption stage is not obvious, SC2 and SC4 only show obvious gasification synergy in the rapid gasification stage, while SC6 and SC8 show gasification synergy in the slow gasification stage and the rapid gasification stage.

https://doi.org/10.1021/acsomega.2c06962
ACS Omega 2023, 8, 6571−6583

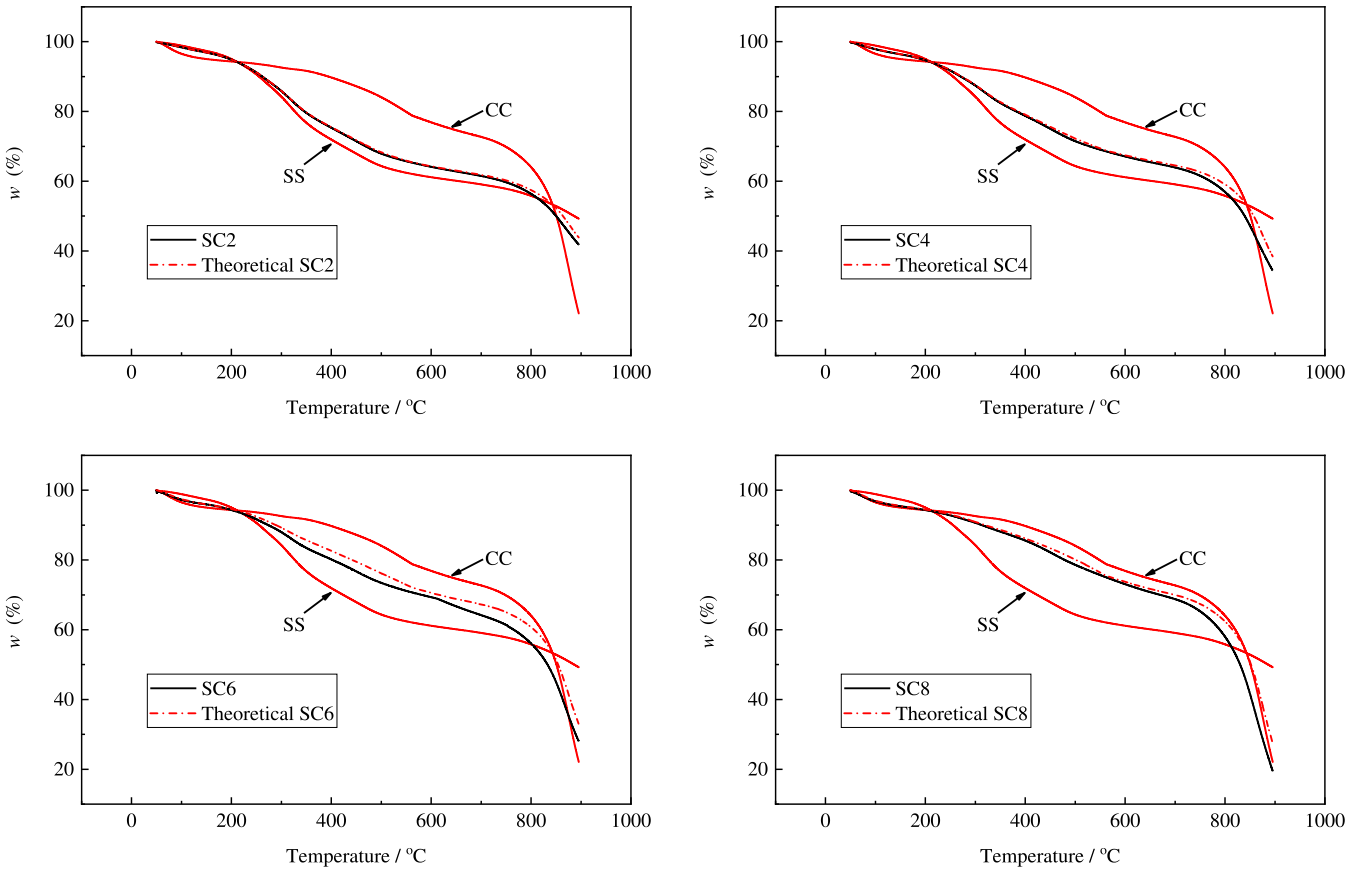

Figure 7. Experimental and theoretical TG curves of samples.

The main reason for this phenomenon is that the reaction temperature in the drying desorption stage is relatively low, and the reaction activity is weak, so there is no significant synergy.

The sludge contains a large number of aliphatic organics, with more phenols (−OH), ethers (−O−CH_2−), carbonyl (C═O), methyl (−CH_3−), methylene (−CH_2−), and subalkyl (−CH(OH)−CH_2−).[31,32] When the reaction enters the slow gasification stage, oxygen-containing functional groups such as phenols and ethers are easy to break chemical bonds during heating. The generated oxygen-containing gas and small molecular groups are in contact with high-sodium coal and adsorbed on the surface of coal particles to promote the fracture of the C−C bond.[33] In addition, functional groups containing more hydrogen such as methyl, methylene, and subalkyl are easy to decompose to form hydrogen-containing gas and small molecular groups when heated. When in contact with high-sodium coal, they may react with free radicals, which can inhibit the polycondensation reaction of coal char to a certain extent and promote the gasification reaction.[34] However, the small proportion of high-sodium coal will lead to the small contact area among the oxygen-containing gas, the hydrogen-containing gas, and small molecular groups produced by sludge heating and coal particles. Therefore, the gasification synergy of SC2 and SC4 is not obvious in the slow gasification stage, while SC6 and SC8 show a relatively significant gasification synergy.

In the rapid gasification stage, the gasification reaction of fixed carbon is mainly carried out. Therefore, the gasification synergy is mainly due to the catalytic effect of heavy metal elements such as Zn, Fe, Ni, Cu, and Mn contained in the sludge on the cracking of macromolecular groups of coal char, which can significantly improve the gasification effect and reduce the yield of coke oil.[35,36]

3.4. Interaction Indexes of Co-Gasification Characteristics. The root-mean-square (RMS) value of relative error was used to describe the degree of the co-gasification interaction, and the RMS was defined as follows

$$\mathrm{RMS} = \sqrt{\left(\sum_{i=1}^{n}((x_{i,e} - x_{i,t})/x_{i,t})^2\right)/n} \tag{12}$$

where $x_{i,e}$ is the experimental value of weight loss, %; $x_{i,t}$ is the theoretical value of weight loss, %; and n is the corresponding number of points on the TG curve.

The RMS value can well reflect the strength of synergy. The larger the RMS value is, the greater the difference between the experimental weight loss and the theoretical weight loss is, the more obvious the synergy is. However, the RMS value cannot determine whether the synergy is a positive promoting reaction or a reverse inhibiting reaction.

Therefore, the mean error (ME) value was used to determine the directionality of synergy. A positive value of ME indicates that the synergy promotes the gasification reaction, while a negative value of ME indicates that the synergy inhibits the gasification reaction. ME was defined as follows

$$\mathrm{ME} = \sum_{i=1}^{n}(x_{i.e} - x_{i,t})/n \tag{13}$$

The RMS and ME values of the samples in the drying desorption stage, slow gasification stage, and fast gasification stage are shown in Figure 8. It can be seen that the RMS values of

https://doi.org/10.1021/acsomega.2c06962
ACS Omega 2023, 8, 6571−6583

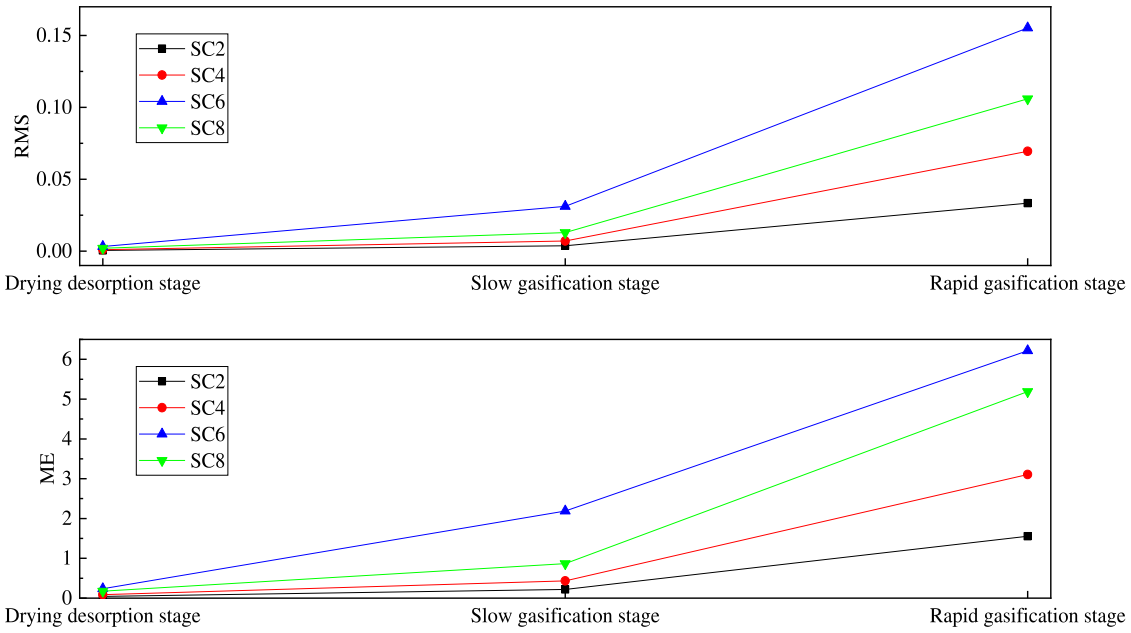

Figure 8. RMS and ME values of the samples.

the samples gradually increase with the progress of the reaction, indicating that the synergy between sewage sludge and high-sodium coal gradually increases with the progress of the reaction. The ME values of the three reaction stages and the whole reaction are positive, indicating that the synergy can positively promote the gasification reaction.

In the drying desorption stage, the RMS value of each sample was small and changes little, indicating that the gasification synergy of sewage sludge and high-sodium coal is not obvious in the drying and desorption stages. However, in the slow gasification stage and the fast gasification stage, the RMS value gradually increases and then decreases with the increase of the coal blending ratio, and both reach the maximum value when the coal blending ratio is 0.6, indicating that the synergistic effect of co-gasification is the strongest at this coal blending ratio, which is consistent with previous research results.

Zou et al.[29] studied the co-gasification of oily sludge and long flame coal and found that the gasification reaction activity was the strongest when the sludge mass ratio was 15%. However, Zhao et al.[37] found that the synergistic effect of co-pyrolysis of sludge and Zhundong coal increased with the increase of the sludge mass ratio. There are some differences in the research results, which may be caused by different reaction conditions, sludge sources, and coal types.

3.5. Kinetic Analysis of Co-Gasification. According to the TGA experimental results at the heating rates of 10, 20, 30, and 40 K·min^{-1}, the linear relationship of ln β and T^{-1} was observed by the OFW method, as shown in Figure 9.

The activation energies corresponding to different gasification conversion rates can be calculated according to eq 6, and the results are shown in Figure 10. According to the calculation results, the gasification reaction activation energy of each sample in the whole conversion range is not a fixed value, but the reaction activation energy basically increases with the increase of conversion in the drying desorption stage, the slow gasification stage, and the fast gasification stage.

The average activation energies of SS, SC2, SC4, SC6, SC8, and CC are 348.94, 343.01, 339.37, 335.45, 345.99, and 358.52 kJ·mol^{-1}, respectively. That is, with the increase of the mass fraction of high-sodium coal in the sample, the average activation energy of the gasification reaction decreases first and then increases. The average activation energy of the SC6 sample is the lowest, which is consistent with previous experimental results, indicating that the co-gasification reaction of sewage sludge mixed with high-sodium coal has significant synergistic characteristics, which can reduce the activation energy of the gasification reaction and improve the gasification reaction rate, but there is the best mixing ratio of high-sodium coal, and the synergistic effect of the co-gasification reaction is the strongest at this coal blending ratio.

It can be inferred that the mixing of sewage sludge and high-sodium coal may have positive and negative effects on the co-gasification reaction: on the one hand, heavy metal elements such as Zn, Fe, Ni, Cu, and Mn in sludge can catalyze the gasification reaction and reduce the activation energy of the gasification reaction process; on the other hand, the mass fraction of ash in sludge is high. With the progress of the gasification reaction, an ash layer will be formed on the surface of fuel particles, which will hinder the contact between fixed carbon and gasification agent and cause partial pore blockage as well as reduce the specific surface area of fuel particles, which is not conducive to the gasification reaction.

Therefore, when co-gasification of sewage sludge and high-sodium coal is carried out, the best mixing ratio needs to be considered.

4. CONCLUSIONS

In the fluidized-bed isothermal co-gasification reaction, as the gasification temperature increased, the CO_2 concentration decreased, and the concentrations of CO and H_2 were increased, while the change of CH_4 concentration was not obvious. As the coal blending ratio increased, the H_2 and CO concentrations initially increased and then decreased, while the CO_2 concentration initially decreased and then increased. In addition, the cold gas efficiency at different temperatures reaches the maximum at the coal blending ratio of 0.6.

In the TGA temperature programmed co-gasification reaction, the whole gasification process can be divided into the

https://doi.org/10.1021/acsomega.2c06962
ACS Omega 2023, 8, 6571−6583

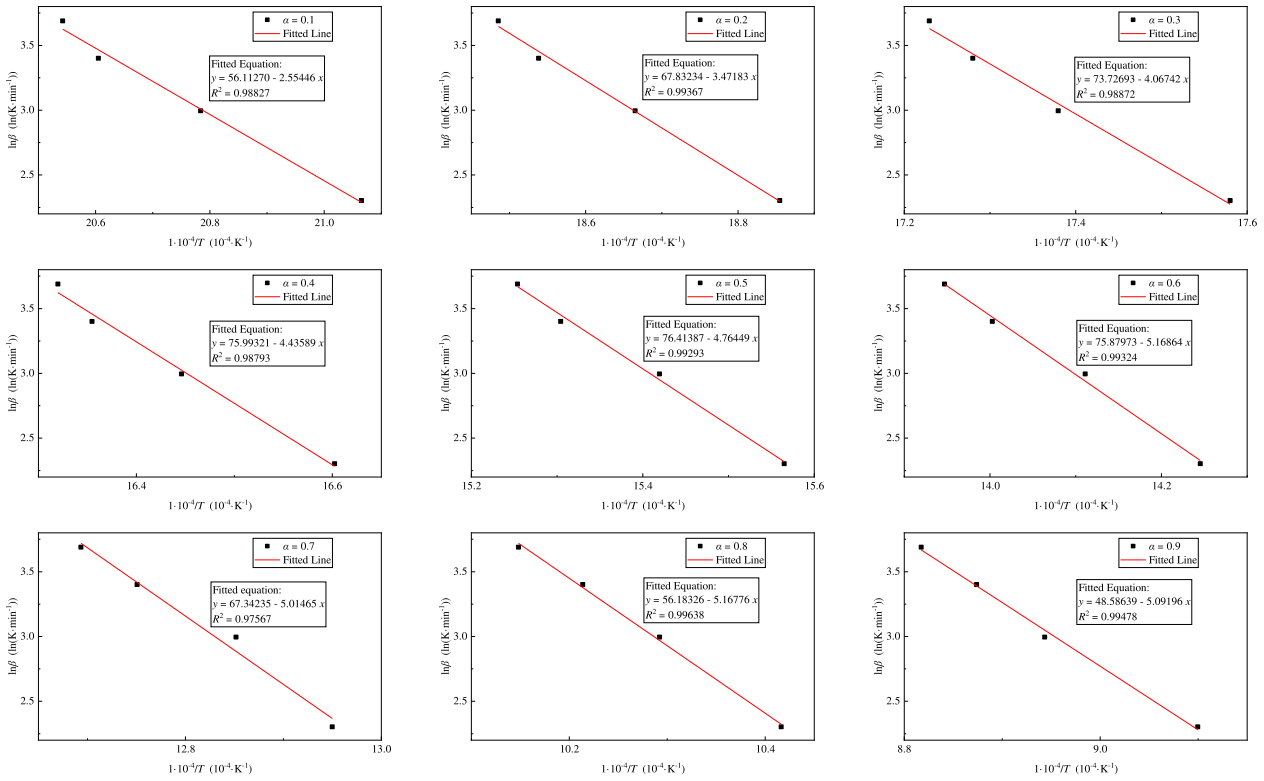

(a) SS

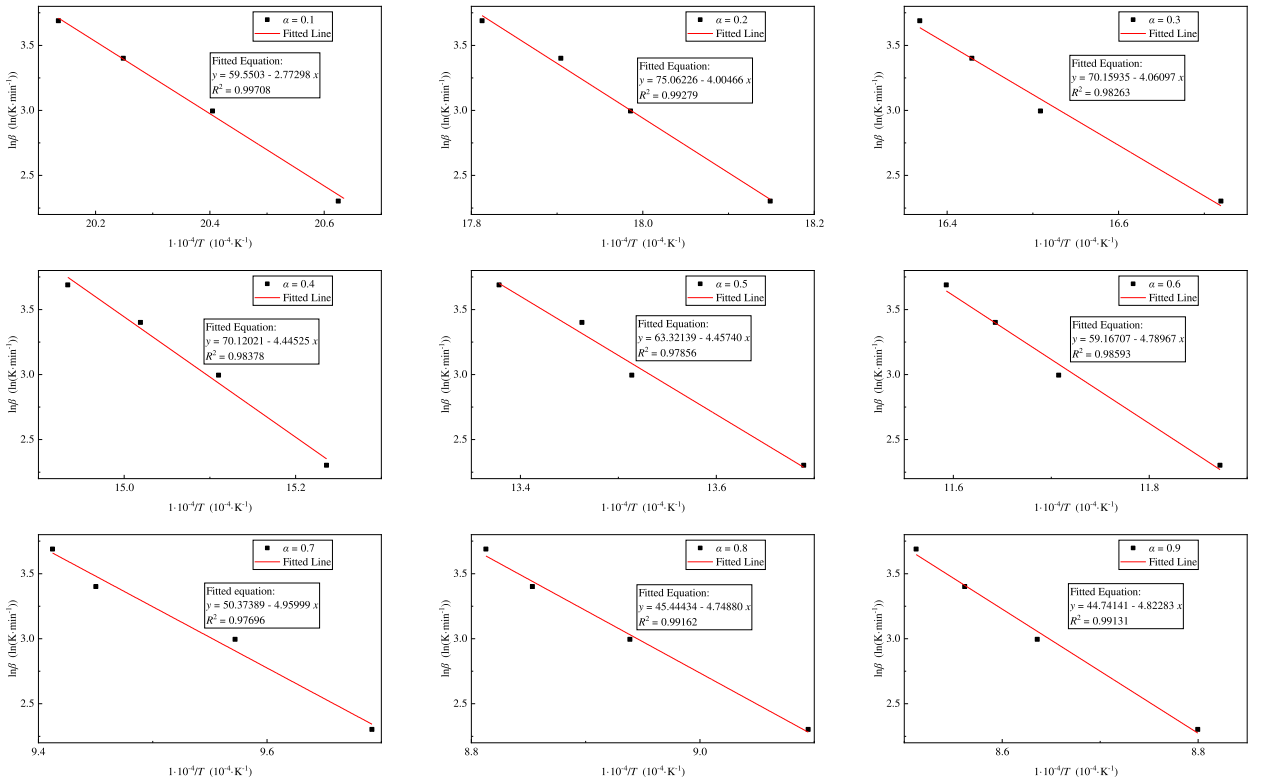

(b) SC2

Figure 9. continued

https://doi.org/10.1021/acsomega.2c06962
ACS Omega 2023, 8, 6571−6583

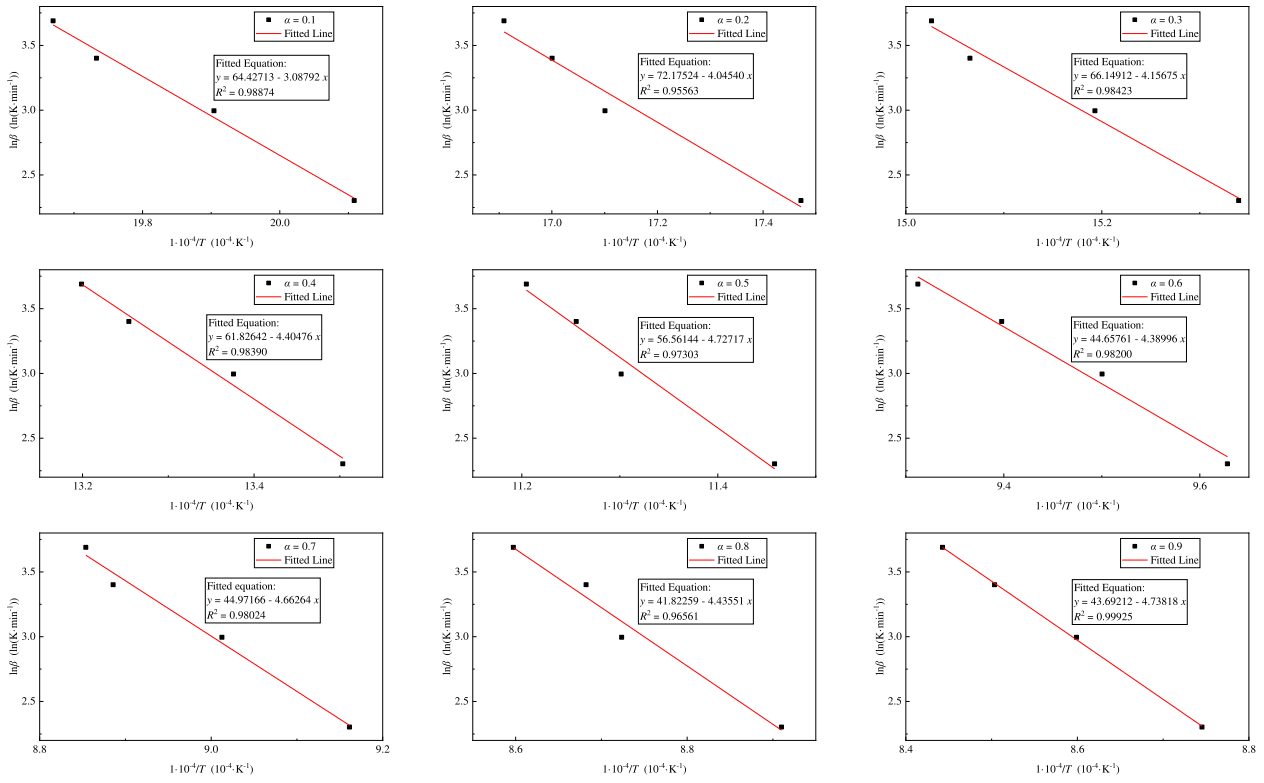

(c) SC4

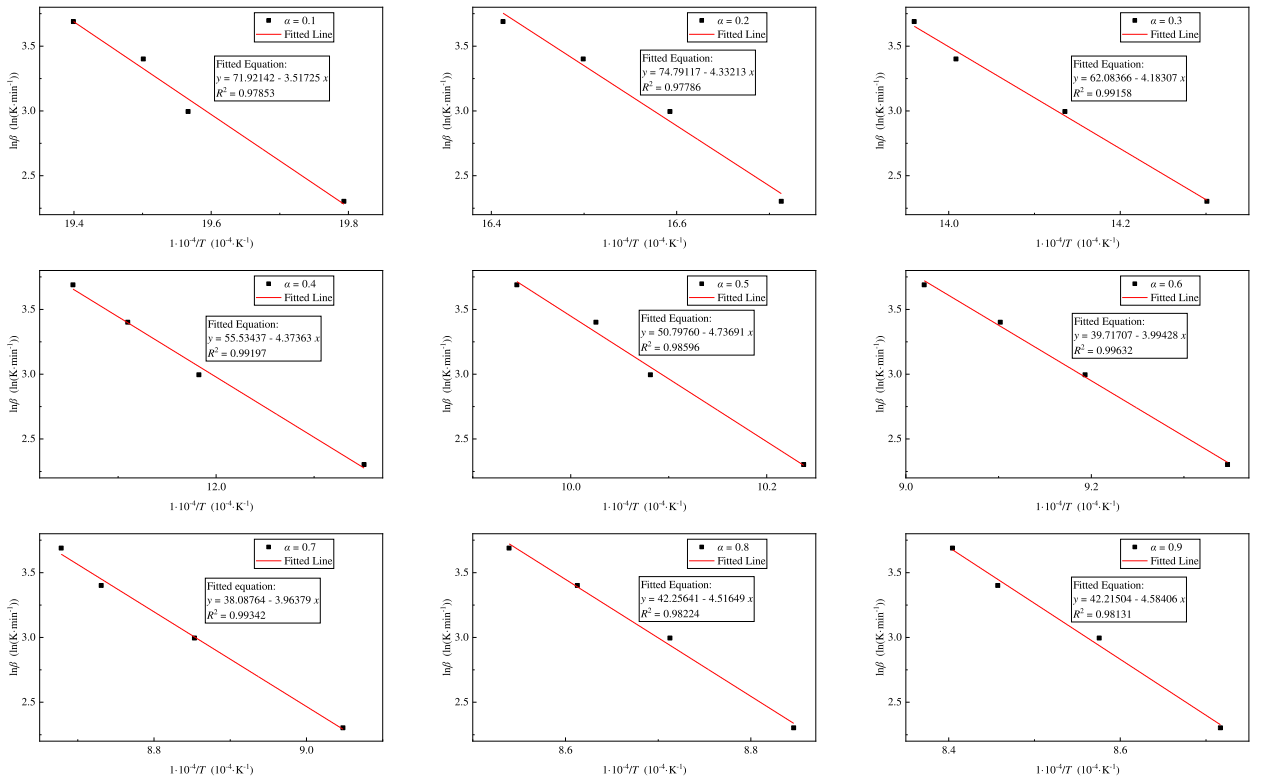

(d) SC6

Figure 9. continued

https://doi.org/10.1021/acsomega.2c06962
ACS Omega 2023, 8, 6571−6583

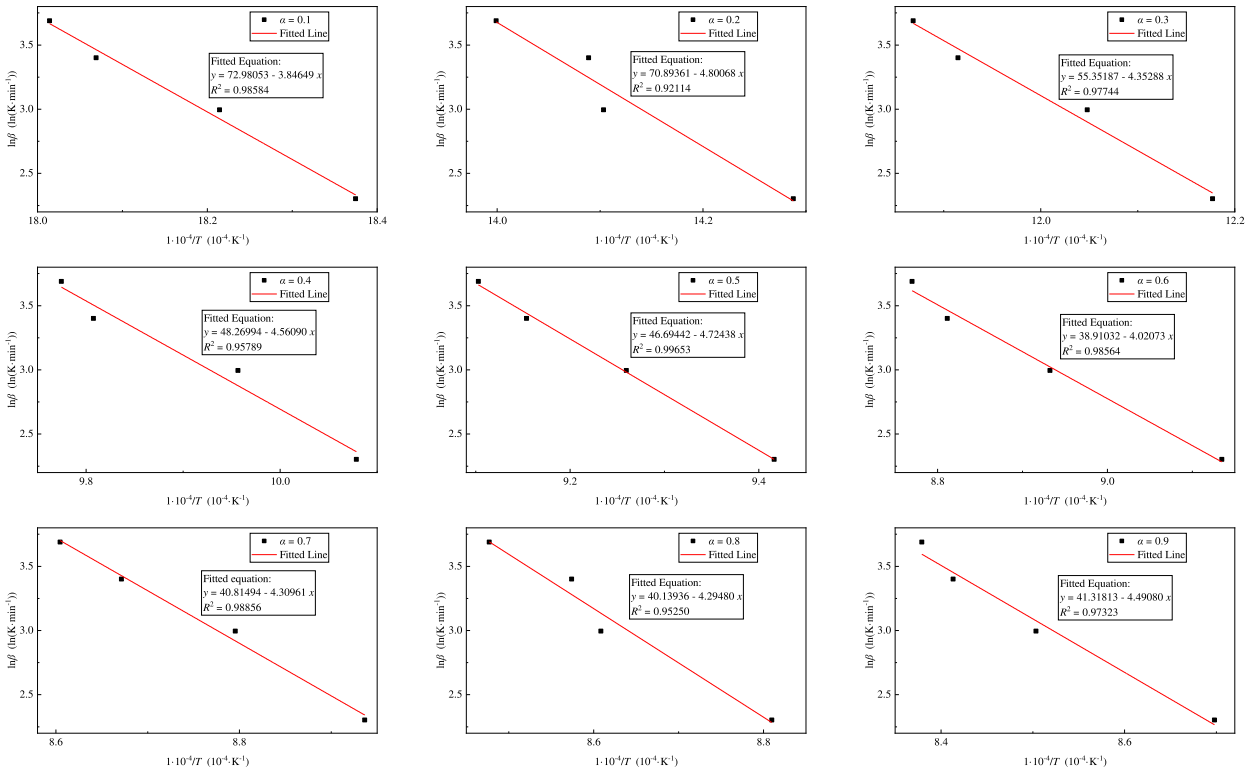

(e) SC8

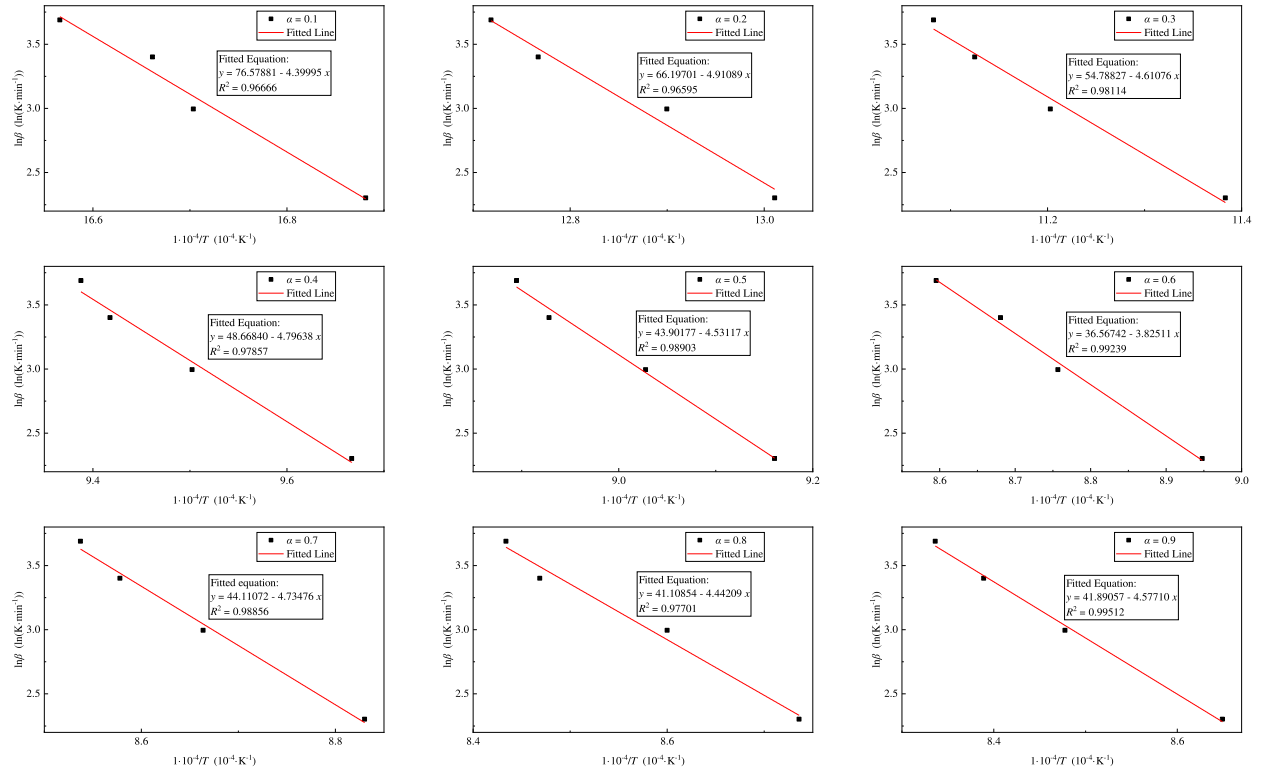

(f) CC

Figure 9. Linear relationship of ln β and T^{-1}: (a) sample of SS, (b) sample of SC2, (c) sample of SC4, (d) sample of SC6, (e) sample of SC8, and (f) sample of CC.

dry desorption stage, the slow gasification stage, and the fast gasification stage. The mixture of sewage sludge and high-sodium coal shows the synergistic effect of co-gasification, and the synergistic effect is to promote the gasification reaction

https://doi.org/10.1021/acsomega.2c06962
ACS Omega 2023, 8, 6571−6583

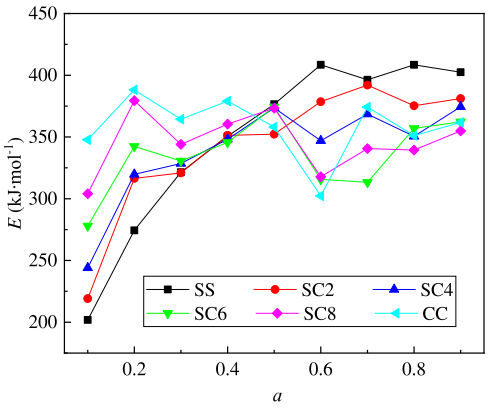

Figure 10. Relationship of activation energy and gasification conversion rate.

positively. The average activation energies of co-gasification reactions were calculated by the OFW method, and the average activation energy first decreases and then increases as the coal blending ratio increases.

Therefore, when sewage sludge and high-sodium coal are subject to temperature programmed or isothermal co-gasification, the best coal blending ratio is 0.6. In addition, due to the different emphasis of the research and the limitation of space, this paper mainly studies the co-gasification synergistic characteristics of sewage sludge and high-sodium coal, while the impact of sodium in high-sodium coal on co-gasification was not studied, which will be carried out in a subsequent research work.

■ ASSOCIATED CONTENT

Data Availability Statement

All data, models, and code generated or used during the study appear in the submitted article.

■ AUTHOR INFORMATION

Corresponding Author

Lilin Zhang − *School of Energy and Architectural Environment Engineering, Henan University of Urban Construction, Pingdingshan 467036, China; School of Energy and Environment, Zhongyuan University of Technology, Zhengzhou 450007, China;* orcid.org/0000-0003-3321-0701; Email: 3533135022@qq.com

Authors

Zhiyuan Zhang − *School of Energy and Architectural Environment Engineering, Henan University of Urban Construction, Pingdingshan 467036, China;* orcid.org/0000-0002-8628-1610

Yin Liu − *School of Energy and Environment, Zhongyuan University of Technology, Zhengzhou 450007, China*

Mingxu Lv − *School of Energy and Environment, Zhongyuan University of Technology, Zhengzhou 450007, China*

Peibo You − *School of Civil and Transportation Engineering, Henan University of Urban Construction, Pingdingshan, Henan 467036, China*

Xutao Wang − *School of Energy and Architectural Environment Engineering, Henan University of Urban Construction, Pingdingshan 467036, China*

Hengtao Zhou − *School of Energy and Architectural Environment Engineering, Henan University of Urban Construction, Pingdingshan 467036, China*

Jing Wang − *School of Energy and Architectural Environment Engineering, Henan University of Urban Construction, Pingdingshan 467036, China*

Complete contact information is available at: https://pubs.acs.org/10.1021/acsomega.2c06962

Notes

The authors declare no competing financial interest.

■ ACKNOWLEDGMENTS

This research was financially supported by the China National Natural Science Foundation Youth Fund Project (52108207), the Science and Technology Project of Henan Province, China (No. 222102320048), the Training Plan for Young Backbone Teachers in Colleges and Universities of Henan Province, China (No. 2021GGJS141), the Key Scientific Research Projects of Universities in Henan Province, China (Nos. 22A480002, 23A480008), the Youth Talent Promotion Projects of Henan Province, China (No. 2021HYTP020), the Science and Technology Guidance Plan Project of Henan Civil Engineering Society, China (Nos. 202121, 202123), and the Academic and Technical Leader Project of Henan University of Urban Construction (No. YCJXSJSDTR202205).

■ REFERENCES

(1) Xiao, Y.; Zhao, R. H.; Chen, J. Fixation of Phosphorus in Ash during Cocombustion of Sewage Sludge and Coals: Influence of Coal and Steam. *Energy Fuels* **2022**, *36*, 4396−4403.

(2) Wang, R. K.; Lin, K.; Peng, P. B.; Lin, Z. H.; Zhao, Z. H.; Yin, Q. Q.; Ge, L. C. Energy yield optimization of co-hydrothermal carbonization of sewage sludge and pinewood sawdust coupled with anaerobic digestion of the wastewater byproduct. *Fuel* **2022**, *326*, No. 125025.

(3) Tong, Y.; Yang, T. H.; Li, B. S.; Song, H. M.; Kai, X. P.; Li, R. D. Transition metal load HZSM-5 catalyst assisted hydrothermal conversion of sewage sludge: Nitrogen transformation mechanism and denitrification effectiveness of bio-oil. *J. Energy Inst.* **2022**, DOI: 10.1016/j.joei.2022.05.009.

(4) Zhang, Z. Y.; Ju, R.; Zhou, H. T.; Chen, H. W. Migration characteristics of heavy metals during sludge pyrolysis. *Waste Manage.* **2021**, *120*, 25−32.

(5) WD, C. U.; Veksha, A.; Giannis, A.; Liang, Y.; Lisak, G.; Hu, X.; Lim, T. Insights into the speciation of heavy metals during pyrolysis of industrial sludge. *Sci. Total. Environ.* **2019**, *691*, 232−242.

(6) Hämäläinen, A.; Kokko, M.; Kinnunen, V.; Hilli, T.; Rintala, J. Hydrothermal carbonisation of mechanically dewatered digested sewage sludge-energy and nutrient recovery in centralised biogas plant. *Water Res.* **2021**, 201.

(7) Wang, R. K.; Lin, K.; Ren, D. M.; Peng, P. B.; Zhao, Z. H.; Yin, Q. Q.; Gao, P. Energy conversion performance in co-hydrothermal carbonization of sewage sludge and pinewood sawdust coupling with anaerobic digestion of the produced wastewater. *Sci. Total. Environ.* **2021**, *803*, No. 149964.

(8) Zhao, Z. H.; Wang, R. K.; Wu, J. H.; Yin, Q.; Wang, C. B. Bottom ash characteristics and pollutant emission during the co-combustion of pulverized coal with high mass-percentage sewage sludge. *Energy* **2019**, *171*, 809−818.

(9) Zha, J. R.; Hang, Y. J.; Clough, P. T.; Dong, L.; Xu, L. G.; Liu, L. Q.; Zhu, Z. C.; Yu, M. Z. Desulfurization using limestone during sludge incineration in a fluidized bed furnace: increased risk of particulate matter and heavy metal emissions. *Fuel* **2020**, *273*, No. 117614.

(10) Eldredge, T. V. The feasibility of solar assisted pyrolysis of sewer sludge and its potential for CO_2 emissions reductions. *Energy* **2021**, *226*, No. 120296.

(11) Kim, D.; Kim, G.; Oh, D. Y.; Seong, K. W.; Park, K. Y. Enhanced hydrogen production from anaerobically digested sludge using microwave assisted pyrolysis. *Fuel* **2022**, *314*, No. 123091.
(12) Migliaccio, R.; Brachi, P.; Montagnaro, F.; Papa, S.; Tavano, A.; Montesarchio, P.; Ruoppolo, G.; Urciuolo, M. Sewage sludge gasification in a fluidized bed: experimental investigation and modeling. *Ind. Eng. Chem. Res.* **2021**, *60*, 5034−5047.
(13) Schmid, M.; Hafner, S.; Biollaz, S.; Schneebeli, J.; Waizmann, G.; Scheffknecht, G. Steam-oxygen gasification of sewage sludge: reduction of tar, H_2S and COS with limestone as bed additive. *Biomass Bioenerg.* **2021**, *150*, No. 106100.
(14) Zhang, Z. Y.; Wang, X. T.; Zhang, L. L.; Zhou, H. T.; Ju, R.; Rao, P. J.; Guo, X. Y.; Han, Y. Q.; Chen, H. W. Characteristics of steel slag as an oxygen carrier for chemical looping gasification of sewage sludge. *Energy.* **2022**, *247*, No. 123534.
(15) Viswanathan, K.; Abbas, S.; Wu, W. Syngas analysis by hybrid modeling of sewage sludge gasification in downdraft reactor: Validation and optimization. *Waste Manage.* **2022**, *144*, 132−143.
(16) Yan, M.; Lin, J.; Kanchanatip, E.; Zhang, S. C.; Wang, G. B.; Hantoko, D.; Wibowo, H.; Hu, Y. J. Influence of Potassic Additives on Sludge Gasification Under Model Flue Gas Atmosphere. *Waste Biomass Valor.* **2020**, *11*, 3629−3637.
(17) Zhang, W. Q.; Chen, J. B.; Fang, H.; Zhang, G. X.; Zhu, Z. B.; Xu, W. H.; Mu, L.; Zhu, Y. Z. Simulation on Co-Gasification of Bituminous Coal and Industrial Sludge in a Downdraft Fixed Bed Gasifier Coupling with Sensible Heat Recovery, and Potential Application in Sludge-to-Energy. *Energy* **2022**, *243*, No. 123052.
(18) Rosha, P.; Ibrahim, H. Technical feasibility of biomass and paper-mill sludge co-gasification for renewable fuel production using Aspen Plus. *Energy* **2022**, *258*, No. 124883.
(19) Szwaja, S.; Poskart, A.; Zajemska, M.; Szwaja, M. Theoretical and Experimental Analysis on Co-Gasification of Sewage Sludge with Energetic Crops. *Energies* **2019**, *12*, No. 1750.
(20) Zhou, H.; Xing, Y.; Zhou, M. Effects of modified kaolin adsorbents on sodium adsorption efficiency and ash fusion characteristics during Zhundong coal combustion. *J. Energy Inst.* **2021**, *97*, 203−212.
(21) Zhang, Z. Y.; Zhou, H. T.; Wang, X. T.; Zhang, L. L.; Rao, P. J.; Zhu, H. G. Influence mechanism of water-soluble sodium on Zhundong coal pyrolysis. *ACS Omega* **2022**, *7*, 11862−11870.
(22) Zhang, Z. Y.; Zhou, H. T.; Zhou, Q.; Rao, P. J.; Zhu, H. G. Catalytic effect of inherently-water-soluble sodium on Zhundong coal gasification. *Sci. Adv. Mater.* **2020**, *12*, 1019−1026.
(23) Vyazovkin, S.; Wight, C. A. Model-free and Model-fitting Approaches to Kinetic Analysis of Isothermal and Nonisothermal Data. *Thermochim. Acta* **1999**, *340−341*, 53−68.
(24) Yan, J. C.; Jiao, H. R.; Li, Z. K.; Lei, Z. P.; Wang, Z. C.; Ren, S. B.; Shui, H. F.; Kang, S. G.; Yan, H. L.; Pan, C. X. Kinetic analysis and modeling of coal pyrolysis with Model-free Methods. *Fuel* **2019**, *241*, 382−391.
(25) Flynn, J. H.; Wall, L. A. A quick, Direct method for the determination of activation energy from thermogravimetric data. *J. Polym. Sci., Part B: Polym. Lett.* **1966**, *4*, 323.
(26) Pinzi, S.; Buratti, C.; Bartocci, P.; Marseglia, G.; Fantozzi, F.; Barbanera, M. A simplified method for kinetic modeling of coffee silver skin pyrolysis by coupling pseudo-components peaks deconvolution analysis and model free-isoconversional methods. *Fuel* **2020**, *278*, No. 118260.
(27) Anyaoha, K. E.; Sakrabani, R.; Patchigolla, K.; Mouazen, A. M. Co-gasification of oil palm biomass in a pilot scale downdraft gasifier. *Energy Rep.* **2020**, *6*, 1888−1896.
(28) Gupta, S.; De, S. An experimental investigation of high-ash coal gasification in a pilot-scale bubbling fluidized bed reactor. *Energy* **2022**, *244*, No. 122868.
(29) Zou, T.; Zhu, C. P.; Zhang, Y.; Lin, Y. A.; Liu, J.; Du, Y. X. Characteristics of microstructures and gasification reactivity of co-pyrolysis coal char with oily sludge and blended coal. *J. Fuel Chem. Technol.* **2020**, *48*, 137−143.
(30) Wang, Q.; Zhao, W. Z.; Liu, H. P.; Jia, C. X.; Li, S. H. Interactions and kinetic analysis of oil shale semi-coke with cornstalk during co-combustion. *Appl. Energy* **2011**, *88*, 2080−2087.
(31) Tsai, W. T.; Lee, M. K.; Chang, J. H.; Su, T. Y.; Chang, Y. M. Characterization of bio-oil from induction-heating pyrolysis of food-processing sewage sludges using chromatographic analysis. *Bioresour. Technol.* **2009**, *100*, 2650−2654.
(32) Lu, Y. J.; Hu, Y. J.; Xu, F.; Yu, W. J. Study on Pyrolysis Mechanism of carbon and oxygen-containing functional groups in sludge by Py-GC/MS. *CIESC J.* **2018**, *69*, 4378−4385.
(33) Shen, T. X.; Zhang, J.; Shen, L. H. Evolution behavior on CO_2 co-gasification of coal and cyanobacteria. *CIESC J.* **2018**, *69*, 5256−5265.
(34) Biagini, E.; Lippi, F.; Petarca, L.; Tognotti, L. Devolatilisation rate of biomasses and coal-biomass blends: an experimental investigation. *Fuel* **2002**, *81*, 1041−1050.
(35) Chen, H.; Lin, C. L.; Zeng, W. Y.; Xu, Z. B. The effect of biomass contents with heavy metal on gasification efficiency during fluidized bed gasification process. *Adv. Mater. Res.* **2012**, *512−515*, 575−578.
(36) Dong, X.; Song, M.; Jin, B.; Zhou, Z.; Yang, X. The synergy effect of Ni-M (M = Mo, Fe, Co, Mn or Cr) bicomponent catalysts on partial methanation coupling with water gas shift under low H_2/CO conditions. *Catalysts* **2017**, *7*, 51.
(37) Zhao, B.; Jin, J.; Li, S.; Liu, D. Y.; Zhang, R. P.; Zhang, H. R. Co-Pyrolysis Characteristics of Sludge Mixed with Zhundong Coal and Sulphur Contaminant Release Regularity. *J. Therm. Anal. Calorim.* **2019**, *138*, 1623−1632.

https://doi.org/10.1021/acsomega.2c06962
ACS Omega 2023, 8, 6571−6583